Development and studies on microstrip detector

V. Radhakrishna, K. Rajanna*, S. S. Desai† and A. M. Shaikh†

Department of Instrumentation, Indian Institute of Science, Bangalore 560 012, India
†Solid State Physics Division, Bhabha Atomic Research Center, Trombay, Mumbai 400 085, India

We report development of gas microstrip detectors using thin film and lithography techniques. The detectors were tested for their performance for X-rays (5.9 keV) and a maximum gas gain of ~13,000 and best resolution of ~12% was obtained. Factors affecting gain and resolution were investigated. The detectors were tested for their one-dimensional position sensitivity. Meandering resistive strips were used for charge division method. A position resolution of 0.48 mm was obtained.

IONIZING radiations play an important role in medicine, biology, materials science and high-energy physics for probing applications and imaging. Gas-filled, semiconductor and scintillation detectors are used widely in these applications with each of them having their own advantages and limitations. The detector technology is evolving rapidly by making use of recent developments in material processing, new detector designs, data acquisition and analysis systems[1].

Amongst gas-filled detectors, Multiwire Proportional Counters (MWPCs) introduced in 1968 by Georges Charpak *et al.*[2] revolutionized the detector technology. Exploiting avalanche multiplication around thin anode wires, the MWPC permits fast detection and localization of charge released in a gas medium by ionizing radiation[3–5]. MWPCs of various designs are major components in detectors for particle physics experiments and their use has also spread in other applied research fields like astrophysics, medical diagnostics, biology, etc.[6,7].

MWPCs are based on thin wires of approximately 10 microns in diameter spaced apart by a few millimeters. Several limitations of MWPCs, such as low rate of detection of radiation and granularity due to the difficulty in stringing together wires closer than a few mms have led the research community to finding out ways to improve them. In this process, several new detector types have been introduced. In 1988, Anton Oed[8] introduced a novel detector, called the Microstrip Gas Chamber (MSGC). MSGCs are found to have superior performance over other conventional detectors such as MWPCs. Comparatively, MSGCs have metallic anode and cathode strips of tens of micron width, generated on insulating substrates using thin film deposition and lithography techniques. Apart from being high resolution neutron detectors in neutron spectrometers[9], MSGCs have found application in spectrometers for synchrotron radiation[10], X-ray astronomy[11], and tracking devices in high-energy physics experiments[12,13]. Invention of MSGC triggered researchers in developing new types of detectors based on micro-fabrication technology. Reviews on various micro-pattern detectors are given in literature[14–16].

We explain here the efforts in developing MSGCs at the Indian Institute of Science, Bangalore using thin film technology and photolithography[17]. Performance of microstrip detectors for X-rays are carried out at BARC, Mumbai and detailed here. Details of various detector characteristics obtained such as gas amplification, energy resolution, energy linearity, position resolution and position linearity are given. Factors affecting the performance are discussed.

Microstrip gas chamber

A cross-sectional view of a general microstrip detector is shown in Figure 1. Referring to Figure 1, one may note that the most important new aspect of microstrip design is that the anode and cathode planes and the closely spaced wires in such planes of the MWPC are replaced by alternating anode and cathode strips of a few microns width deposited in a single plane on a suitable insulating substrate in the MSGC. The applied electric potential alternates between each strip. An electron produced anywhere in the gas volume due to primary ionization travels along the field lines (in drift region) towards the anode and enters the region of high electric field near the anode strips (avalanche region) where it will gain sufficient energy. This energetic electron will produce an avalanche of electrons in the gas medium due to secondary ionization. These secondary electrons move to anodes and the ions drift towards nearby cathodes giving rise to signals on the anode and the cathode strips. In Figure 1 we have shown how signals from each anode and cathode are routed through corresponding electronic systems. As per this scheme, each electrode needs its own electronic detection system. This can, however, be simplified by clever incorporation of a resistive chain along the anodes. The signals can be amplified by external amplifiers and analysed.

A typical microstrip plate designed is shown in Figure 2 schematically. As can be seen in this figure, there are three parts in the designed microstrip pattern. Conducting

*For correspondence. (e-mail: kraj@isu.iisc.ernet.in)

strips are the fine vertical strips that form the main detector part. They contain alternate anodes and cathodes of width of micron dimensions. After several preliminary fabrications of MS plates in our laboratory and based on several tests the design parameters were optimized. The final strips were fabricated with the help of Bharath Electronics Limited (BEL), Bangalore where a good facility to produce quality strips is available. Table 1 shows the design parameters of microstrips prepared with the help of BEL.

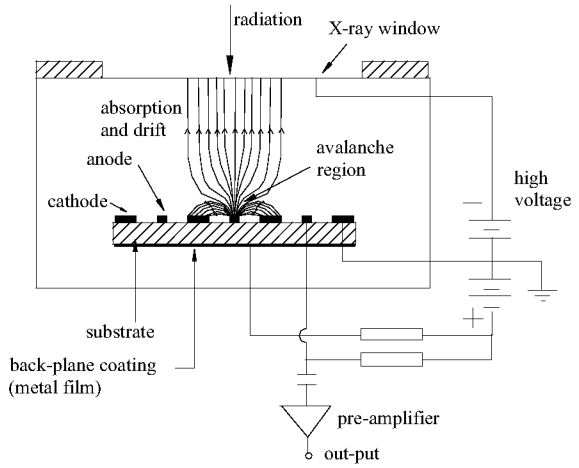

Figure 1. Schematic of the cross-sectional view of MSGC showing working principle of the detector. The anode and cathode strips are normal to the plane of the paper.

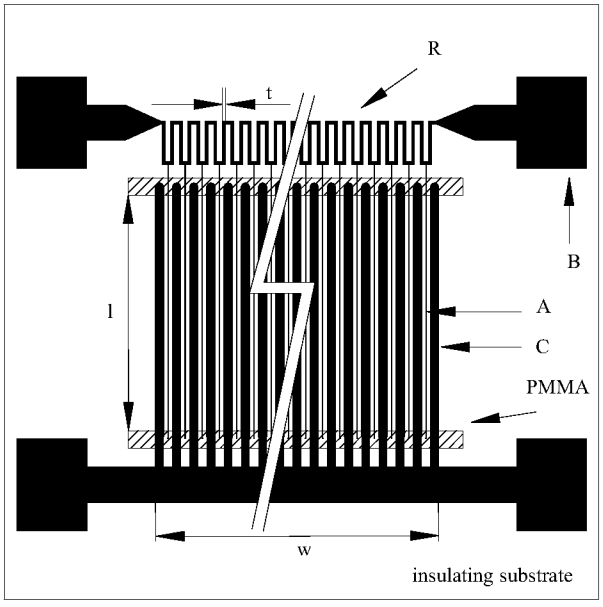

Figure 2. Schematic of the designed microstrip pattern on insulating substrate. A, anode; C, cathode; B, bonding pad; R, meandering resistive strip; t, meandering strip width; PMMA, poly methyl methacrylate coating for end passivation; w, active area width; l, active area length.

When a high potential is applied between the anode and cathode strips, accumulation of charge takes place if the ends of the strips are sharp and pointed. This can cause corona discharge[18], affecting the performance of the microstrip detector. To overcome this problem the ends and corners of the strips are rounded as shown in Figure 3. Also the ends of both anodes and cathodes, shown as shaded region in Figure 2, are coated with poly methyl methacrylate (PMMA) to reduce the discharge[19].

A horizontal strip connects the conducting anodes at one end and this strip has high resistance per unit length compared to that of the anode and cathode strips. High resistance thus provided between any two anode strips aids in position sensing by charge division method. A meandering resistive structure was adopted for this purpose in order to increase the position sensitivity.

The substrate acts as a dielectric medium between the anode and the cathode strips, becoming an active part of the detector and the choice of a suitable substrate has significant influence on the overall performance of the detector. Important properties of the substrate to be considered are: good surface quality and metal adhesion property, moderate surface or bulk resistivity to limit surface charging[20], long term stability of performance and high reliability. Borosilicate glass with surface resistivity of the order of $\sim 10^{15}$ Ω/sq was used in our fabrication.

The material for conducting strips should have high conductivity and good chemical stability. The adhesion

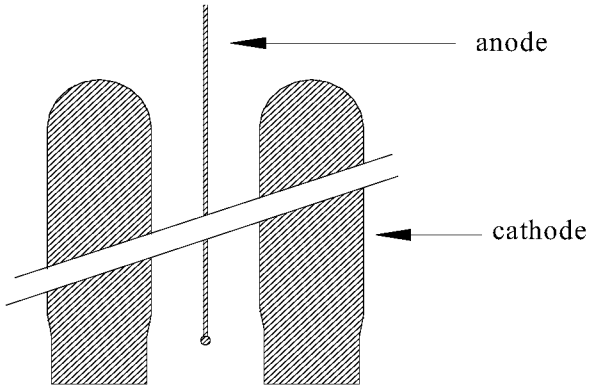

Figure 3. Finer features of microstrip design such as rounded ends and corners of anodes and cathodes.

Table 1. Design parameters of microstrip samples prepared

Substrate	:	Glass-borosilicate
Anode width (μm)	:	12
Cathode width (μm)	:	300
Anode–cathode gap (μm)	:	150
Pitch (μm)	:	612
Active area (mm^2)	:	20×15
Resistive strip width, t (μm)	:	100
Resistive strip resistance	:	44 kΩ

of film material on the substrate must be excellent to protect against accidental release of conducting fragments due to discharge. Most of the metals have their advantages and drawbacks. In the present work chromium has been chosen for the following reasons: It gives good adhesion to the glass substrate, and is one of the sturdiest metals, withstanding mild discharges due to its high melting point.

DC magnetron sputtering has been used for depositing the film. The required pattern for the conducting strips was obtained using photolithography technique. The lift-off lithography method was used to generate bonding pads. The details of thin film deposition and photolithography process are given elsewhere[21].

Performance study

Study of performance of the microstrip detector samples was carried out at Solid State Physics Division, Bhabha Atomic Research Centre, Mumbai. ^{55}Fe, a radio isotope source of X-rays of energy 5.9 keV was used in most of the X-ray measurements. The block diagram of the experimental arrangement used for the observation/measurement of anode pulse is shown in Figure 4. The cathodes were maintained at zero potential. The anode voltage was adjusted to obtain output response from the detector. The microstrip detector works in pulse mode[1]. Each pulse represents the interaction of one quantum of radiation or one particle within the detector active volume. A charge-sensitive pre-amplifier is connected to one end of the anode resistive strips. Figure 5 *a* shows the photograph of pre-amplifier output recorded using the oscilloscope. Output signal of the pre-amplifier is in the range of 50–500 mV with a few exceptions (lowest output ~ 10 mV and highest ~ 1 V) with fast rise time. Linear amplifiers have been used for shaping the signal pulse from the pre-amplifiers. The output pulse (~ 1 V to 10 V) from the amplifier as observed on the oscilloscope screen is shown in Figure 5 *b*. The output of the linear amplifier is fed to a PC-based multichannel analyser (PC-MCA) and the pulse height spectrum was recorded.

A typical pulse height spectrum recorded in PC-MCA is shown in Figure 6. *y*-axis represents counts, i.e. the number of photons as particle detectors and the *x*-axis is the channel number corresponding to pulse height proportional to the X-ray energy absorbed in the detector. This spectrum was recorded for P10 gas, where we see the main peak and the escape peak. Main peak corresponds to 5.9 keV X-ray absorbed in gas medium of the detector. The escape peak is of energy 2.9 keV. These peaks correspond to the pulses shown in Figure 5 *a*, *b*.

From the pulse height spectrum, one can estimate various detector parameters such as its energy resolution, energy linearity, gas gain, etc. Their dependence on the operating conditions like gas composition and pressure, operating voltages, drift gap, back plane voltage, etc. has also been studied. In all the cases, a Gaussian fitted to the pulse height spectral peak is used to evaluate the operating characteristics.

Internal gas amplification or gas gain is one of the major advantages of MSGC and other gas-filled proportional counters over other radiation detectors. Gas gain can be calculated using the formula

$$M = \frac{Q}{Xe}, \tag{1}$$

where M is the gas amplification (gas gain), Q the total charge collected, X the total number of ion pairs produced per photon and e the electron charge which equals 1.6×10^{-19} Coulomb.

The number of ion pairs produced per photon is given by

$$X = \frac{E}{E_{\text{ion}}}, \tag{2}$$

where E, the energy of radiation used = 5.9 keV and E_{ion}, the average energy per ion pair ~ 26.4 eV (for Ar gas).

Hence, $X = 223.48$.

Value of Q is given by

$$Q = VC_{\text{f}}, \tag{3}$$

where V is the pre-amplifier output voltage and C_{f}, the feed back capacitance of pre-amplifier (ORTEC PC142) = 0.5 pf.

Substituting these values in eq. (1),

$$M = \frac{V\,(0.5\times10^{-12})}{223.48\,(1.6\times10^{-19})},$$

$$\text{i.e.} \quad M = V\,(13983). \tag{4}$$

V (in volts) is the pre-amplifier output determined from the peak position of fitted main peak of the pulse height spectrum, where channel number along *x*-axis is calibrated with amplifier output (in volts) as shown in Figure 5 *b*.

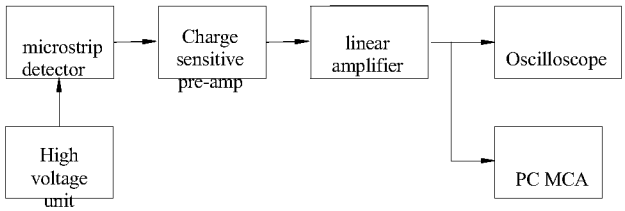

Figure 4. Block diagram of experimental arrangement used to record anode pulse height spectra.

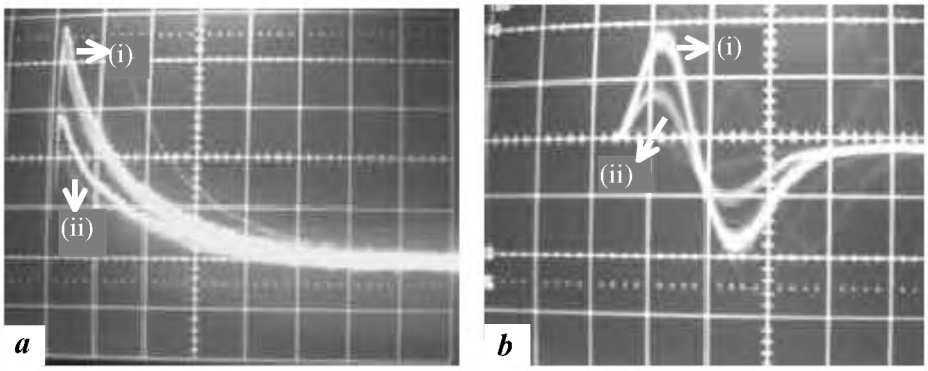

Figure 5. *a*, Pre-amplifier output pulses observed on the oscilloscope; *b*, Linear amplifier output pulses observed on the oscilloscope. The two pulses (i) and (ii) in (*a*) and (*b*), correspond to X-ray photons of energy 5.9 keV (main peak) and 2.9 keV (escape peak) respectively.

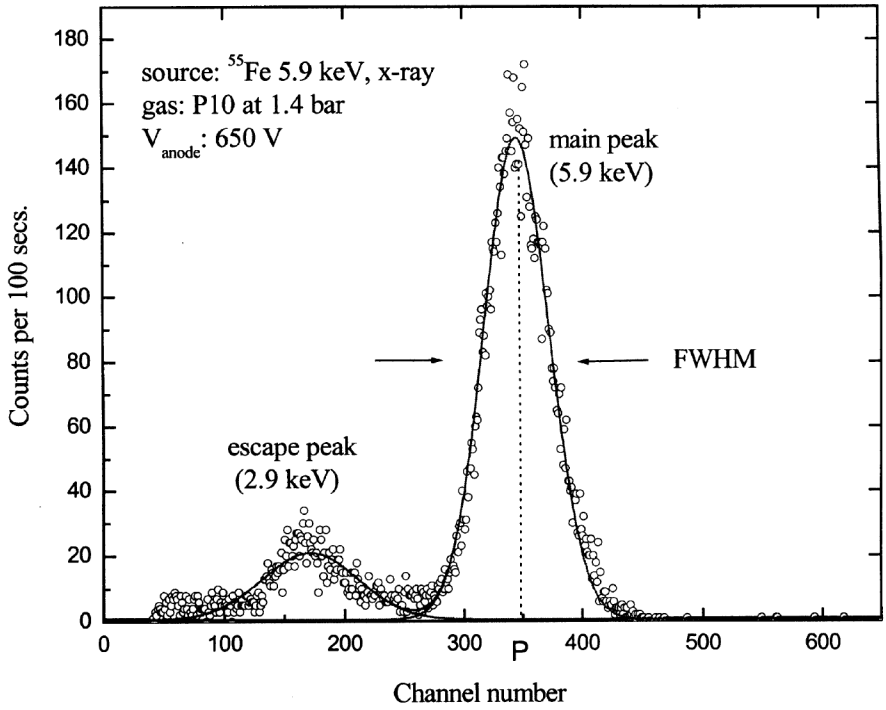

Figure 6. Typical pulse height spectrum recorded for P10 gas using PC-MCA corresponding to pulses shown in Figure 5. Solid line is the Gaussian fit.

In some applications of the detectors, the main objective is to measure the energy distribution of the incident radiation as in X-ray astronomy. The ability of a detector to resolve fine details in the incident energy spectrum of radiation is termed as energy resolution.

Energy resolution is defined as

$$\text{Energy resolution} = \frac{\Delta E}{E_{\text{peak}}}, \tag{5}$$

where ΔE is the full width at half maximum (FWHM) of the peak in the pulse height spectrum and E_{peak} the energy corresponding to the peak position in that spectrum.

However, the width or dispersion reflects the fact that certain fluctuation in pulse height was recorded from pulse to pulse, even though the same amount of energy is deposited in the detector for each event. The factors affecting the energy resolution are the collection efficiency of primary electrons, the gas gain fluctuations and the non-uniformity of the gas gain. By choosing proper design parameters and operating parameters/conditions we can control the above factors. The quality of microstrip in its strip edge uniformity affects the energy resolution[22].

Pulse height spectrum recorded for ^{57}Co isotopic source is shown in Figure 7 *a*. ^{57}Co, a γ source, decays into ^{57}Fe, which emits characteristic X-rays at 14.41 keV

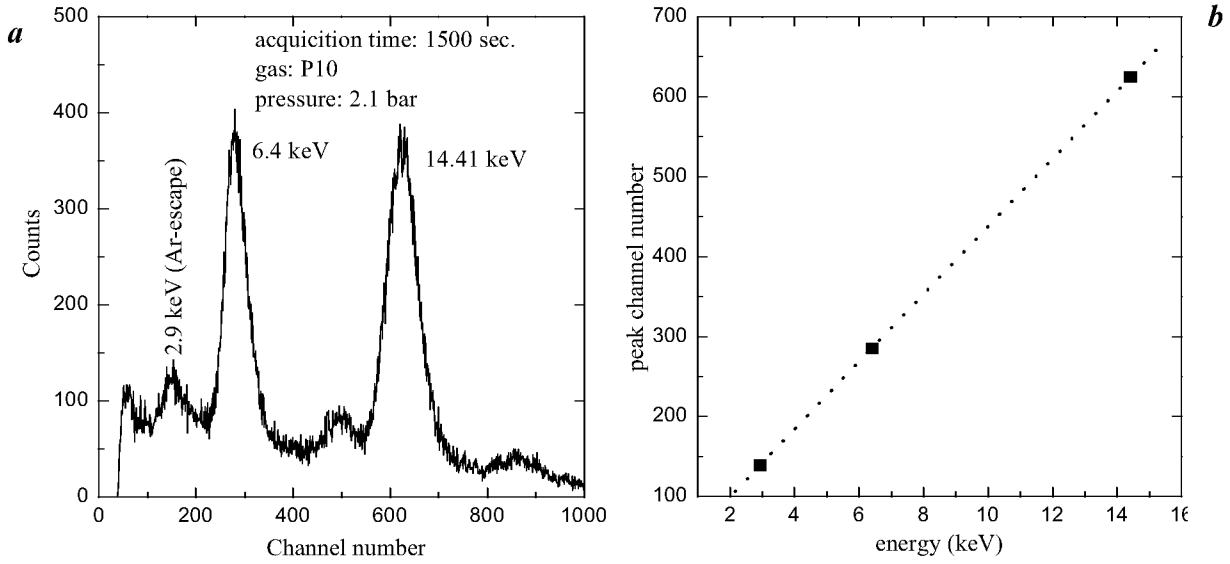

Figure 7. *a*, Pulse height spectrum of ^{57}Co source; *b*, Energy linearity curve.

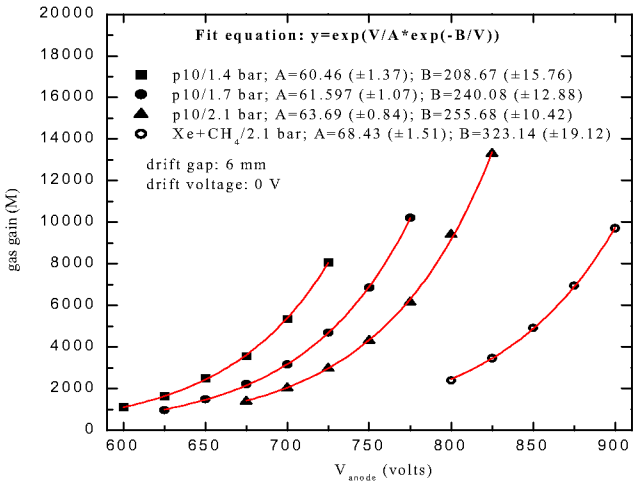

Figure 8. Variation of gas gain with increasing anode voltage at different gas pressures. The lines through the experimental points are fits to the expression given in the figure.

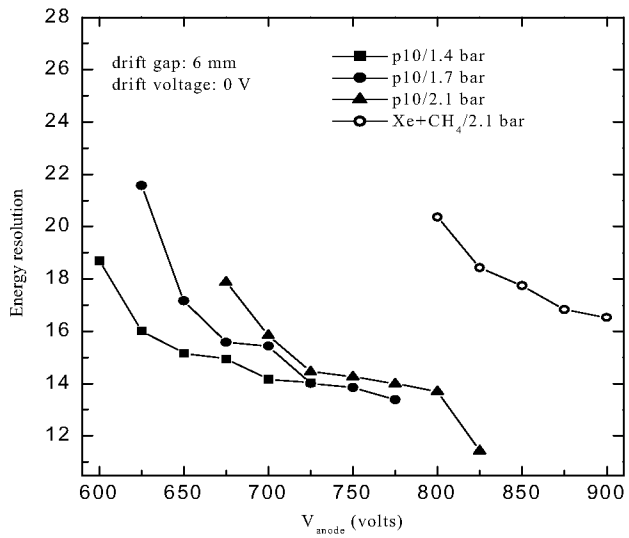

Figure 9. Variation of energy resolution with increasing anode voltage at different gas pressures.

and 6.4 keV. In addition to these two peaks, an argon escape peak corresponding to 2.93 keV is also present. Figure 7 *b* shows the nature of relation between energy deposited and the peak channel numbers. It may be noted that the relation is a good linear one.

The microstrip detectors were tested for varying anode voltages. In these cases the cathode potential was maintained at 0 V. Tests were carried out without applying the back plane voltage. A drift gap of 6 mm was maintained during the measurements. Anode voltage was increased in steps of 25 V. The maximum voltage was restricted to a value when one can notice discharge precursors starting to appear in the oscilloscope.

The variation in gas gain with anode voltage measured is given in Figure 8. The gas gain was calculated as described earlier, for different anode voltages.

An empirical formula for gain value is given as[23]

$$M = \exp\left(\frac{V}{A}\exp\left(-\frac{B}{V}\right)\right), \tag{6}$$

where M is the gas gain, V – the anode–cathode potential, A and B are constants which depend on field geometry, the ambient variable pressure (P) and temperature (T) and the atomic properties of the gas mixture (ionization cross-section, etc.). As can be seen, this equation fits all the curves in Figure 8. Ideally the variables A and B are dependent only on the gas and the dimensions of the strip pattern. In the present work a maximum gain of ~13,000 was obtained for P10 gas at 2.1 bar pressure.

Energy resolution of the detector depends on the anode voltage as shown in Figure 9. The resolution improves

with the increase in anode voltage, as the amplification is limited to smaller region on the microstrip at higher electric field value. FWHM varies inversely with square root of gas gain, M (ref. 22). A best resolution of ~12% was obtained for P10 gas at 2.1 bar pressure.

MSGC as one-dimensional position-sensitive detector

One advantage of MSGCs over other conventional gas ionization-based detectors is their better position resolution. This is achieved due to the small spacing between the anode and the cathode strips. In this section, some of the basic properties of a position-sensitive detector (PSD) and development and study of MSGC as a PSD are discussed. Experimental study was carried out to determine the effect of operating parameters on the position resolution. The MSGC was studied in one-dimensional mode.

Resistive electrodes have been used for position sensing in proportional counters[24] and also in semiconductor detectors. Basically there are two methods for position sensing using resistive electrodes. In 'charge division method', the position is determined from the ratio of charge flowing out of the ends of resistive electrode terminals. In the second method called 'rise time method', the position is determined from the difference in the signal diffusion time from the point where the charge is collected. A third read-out technique is the one based on 'multielectrode technique' (in case of MSGCs each strip is an electrode) where one amplifier per electrode is used. Charge division read-out method adopted in PSD applications, simplifies the electronics to use only two sets of pre-amplifiers and amplifiers. We report here a study on microstrip-based PSD employing charge division read-out method.

Charge division read-out in MSGC

The process of charge division in a microstrip plate is shown in Figure 10. Let us assume that an avalanche reaches the point P on one of the anodes. The charge induced by the avalanche reaches a corresponding point Q on the meandering resistive strip without much loss instantaneously. This charge reached at point Q on the resistive anode strip is divided into two streams Q_a and Q_b and flows in two opposite directions. The amount of charge flowing in one direction is inversely proportional to the resistance of that segment of resistive strip, i.e. x or $(l - x)$ but is independent of total resistance. Charge-sensitive pre-amplifiers at both ends of the resistive anode generate two signals V_a and V_b for each detected particle or photon.

From Figure 10 it can be noted that

$$V_a \propto \tilde{n}(l-x)+z,$$

$$V_b \propto \tilde{n}x+z,$$

$$\frac{V_b}{V_a+V_b} = \frac{\tilde{n}x+z}{\tilde{n}l+2z} \tag{7}$$

$$= \frac{\tilde{n}x}{\tilde{n}l} \text{ for } (z << \tilde{n})$$

$$= \frac{x}{l}. \tag{8}$$

Here z is the input impedance of pre-amplifier and ρ the resistivity of resistive strip material. The equation shows that the output $V_b/(V_a + V_b)$ is proportional to positional coordinate x of the point Q (ref. 25).

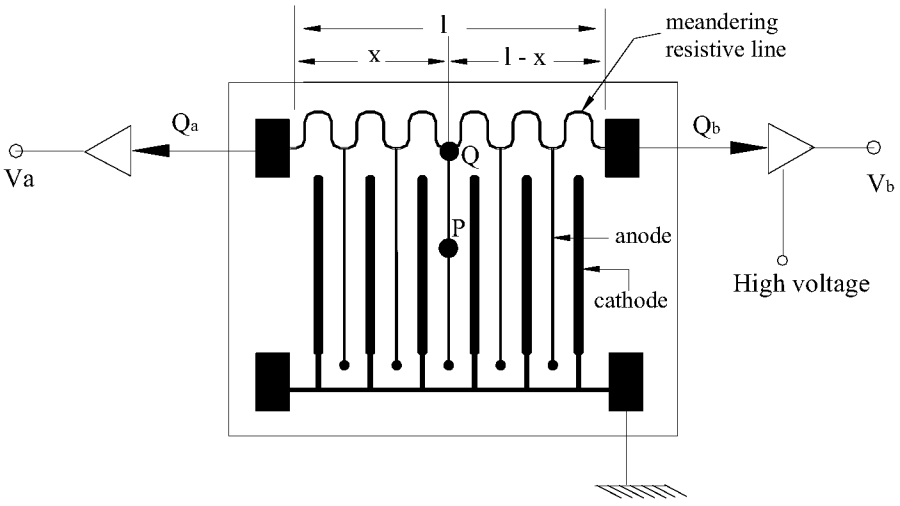

Figure 10. Schematic showing charge division principle in MSGC.

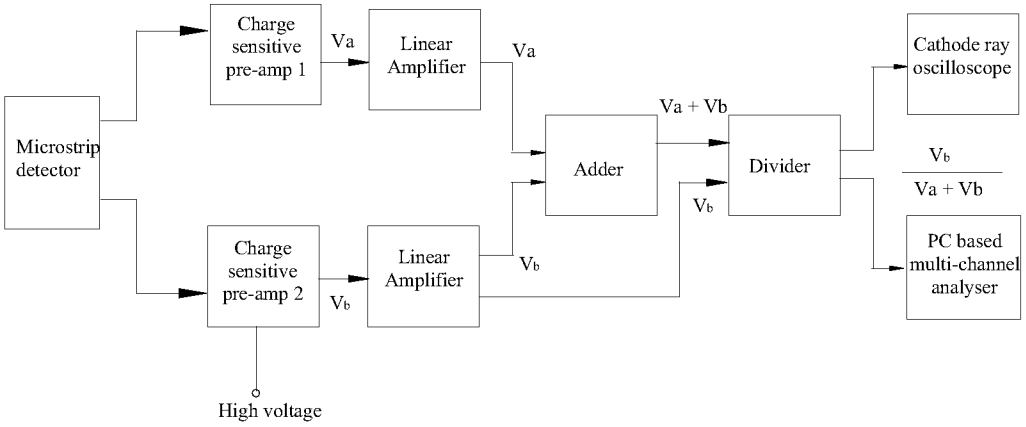

Figure 11. Block diagram of experimental set-up used for one-dimensional position-sensitive measurement using charge division method.

In this work, meandering structure for the resistive strip has been adopted, which enabled increase of resistance between successive anodes. This, in fact, has the same effect as that of using higher resistivity material. Resistive strip material used is the same as that used for conducting strips. This has the added advantage of simplicity of design and fabrication and can be made in one-stage lithography process. Due to the meandering structure it is possible to vary the resistance easily by changing the width or length of meandering in the design. Uniformity of the resistance between successive anodes can be maintained due to the accuracy in lithography technology.

The block diagram of the experimental set-up used for position-sensitive detector based on charge division method, is shown in Figure 11. The two output signals from pre-amplifiers V_a and V_b form inputs to corresponding linear amplifiers. The two output signals from the linear amplifiers are added using an adder to give $(V_a + V_b)$. V_a or V_b and $(V_a + V_b)$ are then fed to a pulse divider. The divider output, namely, $V_b/V_a + V_b$ is then fed to PC-MCA for recording the position spectrum.

The signal processing in resistive method of position encoding like charge division technique is critical in order to achieve the best position resolution, linearity of the output signal with the particle position and to maximize the count rate.

A pulsar was used to adjust the gain of pre-amplifiers and amplifiers at both ends of the detector. The output pulses from the two linear amplifiers, V_a and V_b from two ends of anode-resistive strips were made equal by adjusting the gains of the linear amplifiers.

To determine if position sensitivity is linear, the X-ray beam from ^{55}Fe source was collimated using a slit collimator, 150 μm wide × 10 mm long and the active area of the microstrip was scanned across through the centre. Schematic of the experimental arrangement is shown in Figure 12. The source along with the collimator was mounted on a carriage, which could be traversed by means of a micrometer screw across the chamber in a

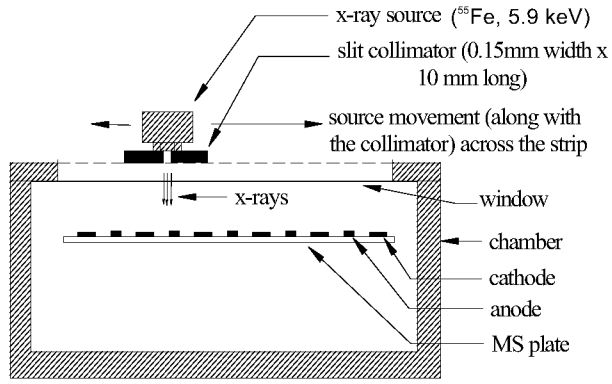

Figure 12. Schematic of experimental arrangement for recording position spectra at different source-collimator positions.

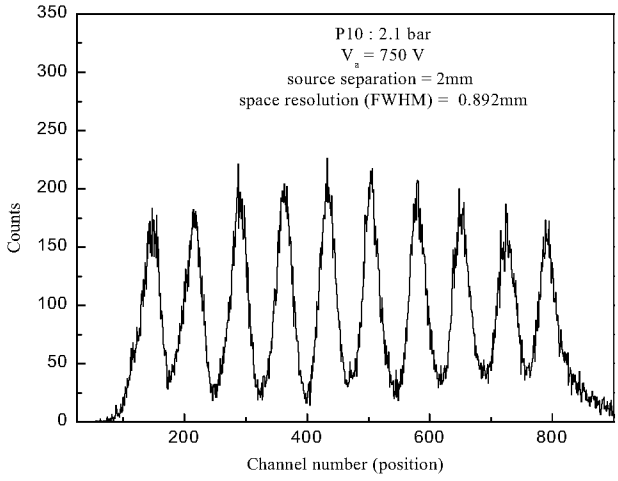

Figure 13. Position spectrum recorded for different source-collimator positions. Separation between successive positions: 2 mm.

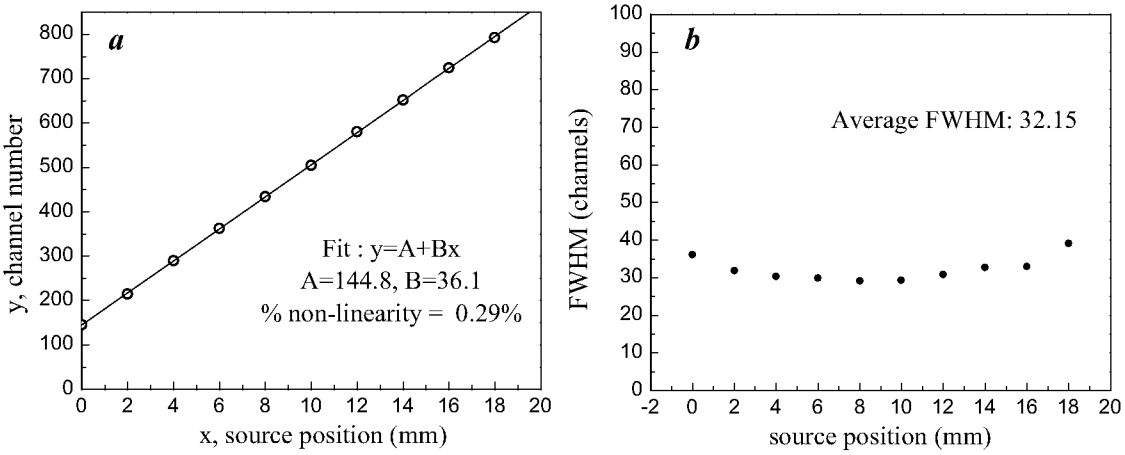

Figure 14. *a*, Position linearity graph: peak channel against X-ray source position from Figure 13; *b*, Uniformity of FWHM space resolution across the microstrip.

direction perpendicular to the strips to change the source position.

The position spectrum recorded is shown in Figure 13. This was recorded for a gas mixture of P10 at 2.1 bar pressure. The drift gap was 6 mm. The operating voltage (V_{anode}) was 750 V and the drift voltage was maintained at 0 V. The spectrum was recorded using a PC-MCA at successive source positions of 2 mm.

The peak position (channel number) versus the position of source for the spectrum in Figure 13 is shown in Figure 14 *a*. It can be observed that over a distance of 18 mm, through the centre of the detector, a linear relation is observed with a maximum deviation of 0.29%. The slope of the curve is a measure of the sensitivity of the detector. The value of the slope, 36 channels/mm, indicates very good sensitivity. These results clearly demonstrate usefulness of the meandering strip structure adopted for the resistive strip especially for detectors with lower rate applications. The uniformity of FWHM space resolution as a function of position across the anode strips is also shown in Figure 14 *b*.

The position resolution in length scale for any position spectrum recorded is

$$\text{Position resolution (FWHM) in mm} = \frac{\text{Source separation for two peaks (mm)}}{\text{Distance between two peak positions (channels)}} \times \text{FWHM (channels)}. \quad (9)$$

In the present study, the position spectra are recorded for different operating conditions. The ultimate spatial resolution obtained is derived from Figure 15 and is equal to 0.487 mm. This resolution was recorded for $Xe + CH_4$ gas at 2.1 bar pressure. It can be noted that, the slit collimator used was of 0.152 mm width.

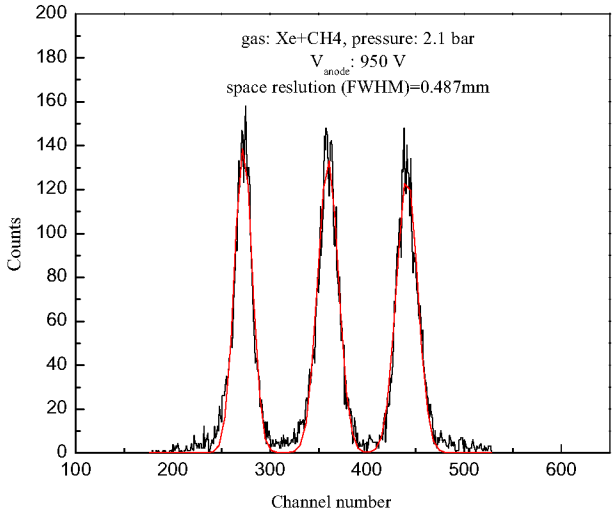

Figure 15. Position spectrum recorded at three different source positions 2 mm apart.

There are many operating parameters and conditions, which influence the position resolution of the detector. The electrons and ions generated due to ionization drift towards the electrodes. The electron cloud moving towards the anode plane undergoes avalanche multiplication due to quadrupole field giving rise to signal on to a few anode strips. The position of the incident particle beam is determined from the pulse induced on all these strips. The position resolution of MSGC and other gas ionization-based detectors is influenced by effects[26,27] such as range of delta-electrons, gain fluctuation, transverse diffusion of primary electron cloud and electronic noise.

The position resolution depends on the precision of the relative signal measurement at the two ends of resistive electrode, i.e. the signal-to-noise ratios of the two measurements. Position resolution is given by[28],

$$\frac{\Delta l}{l} = 2.54\frac{\sqrt{kTC_D}}{Q_s} \text{ FWHM.} \quad (10)$$

Q_s is the total charge generated by the incident particle.

Position spectrum was recorded for different anode voltages. A maximum anode voltage is set by a value where a discharge precursor starts appearing. The FWHM variation with varying anode voltage is shown in Figure 16. The space resolution improves with increasing anode voltage. As the anode voltage is increased, the gain of the MS detector increases. This implies that the total charge produced, Q_s, increases with anode voltage; hence the FWHM decreases as given by eq. (10).

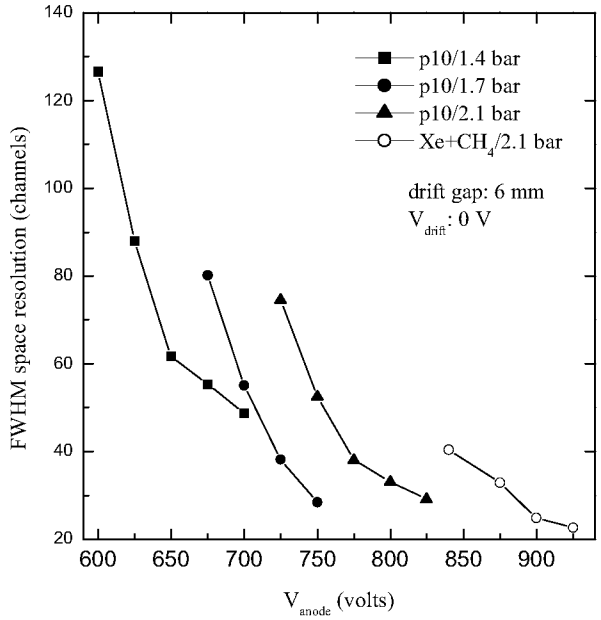

Figure 16. Space resolution, FWHM variation with anode voltage at different gas pressures.

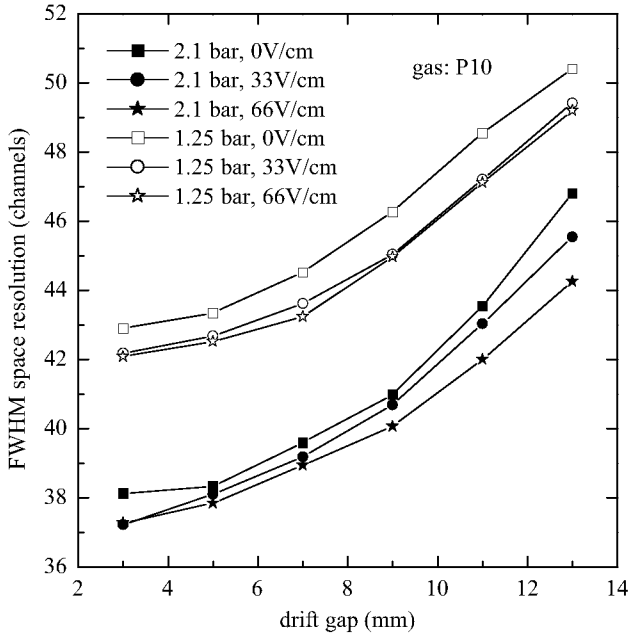

Figure 17. Variation of FWHM space resolution with drift gap at different gas pressures and different drift field values for P10 gas.

The variation of FWHM of space resolution with changing drift gap at different gas pressures for P10 are given in Figure 17. The experiment was carried out at different drift field values. The increase in FWHM is due to the combined effect of electronic noise, statistics and diffusion of electron cloud. However, the dominating factor would be diffusion of electron cloud[29].

The spread with time of an originally point-like charge is described by a field-dependent diffusion coefficient D. The rms spread due to the diffusion along any direction, at time t is given by[30]

$$\sigma_d = \sqrt{2Dt} = \sqrt{\frac{2\varepsilon_k x}{eE}} = \sqrt{\frac{2\varepsilon_k x}{e(Ep^{-1})}}\frac{1}{\sqrt{p}}, \quad (11)$$

where ε_k is the characteristic energy of the electron, p the gas pressure, E the drift field, x the drift gap and Ep^{-1} the reduced electric field. One can see that the diffusion depends not only on E or Ep^{-1} but also on $1/\sqrt{p}$. Apart from electric field and gas pressure, drift gap x plays an important role in the position resolution and hence optimization of the same is essential.

In conclusion, it may be noted that the design and development of microstrips reported in this note is the first effort in our country for the realization of a high spatial resolution detector that can be used for detection of charged particles, neutrons or photons depending on the fill gas used in the microstrip chamber. Feasibility of fabrication of such detectors and its characterization has been established by this work. However, experimentalists have yet to adopt such detectors for various experiments in physics or imaging in the country. These detectors can also be used as 2-D detectors (for area detectors) by slight modifications of microstrips.

1. Knoll, G. F., *Radiation Detection and Measurement*, John Wiley, 1979.
2. Charpak, G., Bouclier, R., Bressani, T., Favier, J. and Zupancic, C., *Nucl. Instrum. Methods*, 1968, **62**, 262.
3. Sauli, F., *Technical Rep.*, CERN 77-09, 3 May 1977.
4. Charpak, G. and Sauli, F., *Nucl. Instrum. Methods*, 1973, **113**, 381.
5. Souder, P. A., Sandweiss, J. and Disco, D. A., *Nucl. Instrum. Methods*, 1973, **109**, 237.
6. Sauli, F., *Rad. Protect. Dosimetry*, 1995, **61**, 29.
7. Neumann, M. J. and Nunamaker, T. A., *IEEE Trans. Nucl. Sci.*, 1970, **NS-17**, 43.
8. Oed, A., *Nucl. Instrum. Methods*, 1988, **A263**, 351.
9. Clergeau, J. F. *et al.*, *Nucl. Instrum. Methods*, 2001, **A471**, 60.
10. Ochi, A., Aoki, S., Nishi, Y. and Tanimori, T., *Nucl. Instrum. Methods*, 1997, **A392**, 124.

11. Carl Budtz-Jorgensen, Bahnsen, A., Olesen, C., Madsen, M. M., Johnasson, P., Schnopper, H. W. and Oed, A., *Nucl. Instrum. Methods* 1991, **A310**.
12. de Groot, N. *et al.*, Proceedings of the MSGC Workshop, Lyon, 1995, p. 137.
13. Blouw, J. *et al.*, Proceedings of the MSGC Workshop, Lyon, 1995, p. 143.
14. Sauli, F. and Sharma, A., *Annu. Rev. Nucl. Part. Sci.*, 1999, **49**, 341.
15. Oed, A., *Nucl. Instrum. Methods*, 2001, **A471**, 109.
16. Sauli, F., CERN-EP/1999-147.
17. Radhakrishna, V., Ph D thesis, Department of Instrumentation, Indian Institute of Science, 2002.
18. Angelini, F., Bellazzini, R., Brez, A., Massai, M. M., Spandre, G. and Torquati, M. R., *Nucl. Instrum. Methods*, 1989, **A283**, 755.
19. Bellazzini, R., Brez, A., Latronico, L., Lumb, N., Spandre, G., Bozzo, M., Cattai, A. and Tsirou, A., *Nucl. Instrum. Methods*, 1997, **A398**, 426.
20. Bouclier, R., Million, G. and Ropelewski, L., *Nucl. Instrum. Methods*, 1993, **A332**, 100.
21. Radhakrishna, V., Rajanna, K., Desai, S. S. and Shaikh, A. M., *Rev. Sci. Instrum.*, 2001, **72**, 1361.
22. Bateman, J. E., Connolly, J. F., Derbyshire, G. E., Duxbury, D. M., Mir, J. A., Spill, E. J. and Stephenson, R., RAL-TR-2000-022.
23. Bateman, J. E., *RAL Rep.*, RAL-TR-1998-044.
24. Radeka, V., *IEEE Trans. Nucl. Sci.*, 1974, **21**, 51.
25. Miller, G. L., Williams, N., Senator, A. and Stensgaard, R., *Nucl. Instrum. Methods*, 1971, **91**, 381.
26. Vermeulen, J. C., *Nucl. Instrum. Methods*, 1981, **185**, 591.
27. Schmitz, J., *Nucl. Instrum. Methods*, 1992, **A323**, 638.
28. Radeka, V. and Rehak, P., *IEEE Trans. Nucl. Sci.*, 1979, **26**, 225.
29. Filatova, N., Nigmanov, T., Pugachevich, V., Riabtsov, V. and Shafranov, M., *Nucl. Instrum. Methods*, 1977, **143**, 17.
30. Sauli, F., *Nucl. Instrum. Methods*, 1978, **156**, 147.

ACKNOWLEDGEMENTS. The work reported in this paper has been supported by the Board of Research in Nuclear Sciences (BRNS), Department of Atomic Energy, India, through a research project. We acknowledge the support of Dr K. Natarajan, Bharath Electronics Ltd, Bangalore for his help in getting microstrip plates fabricated. Respectful thanks are due to Dr K. R. Rao (Ex-Director, Solid State and Spectroscopy Group, BARC) for his interest and many useful discussions and suggestions during the course of the work

Received 7 December 2002; revised accepted 1 March 2003